Chemical Science

ROYAL SOCIETY OF CHEMISTRY

EDGE ARTICLE

View Article Online
View Journal | View Issue

Cite this: *Chem. Sci.*, 2022, **13**, 3395

All publication charges for this article have been paid for by the Royal Society of Chemistry

Stepwise assembly and reversible structural transformation of ligated titanium coated bismuth-oxo cores: shell morphology engineering for enhanced chemical fixation of CO_2†

Qing-Rong Ding,[ab] Yinghua Yu,[a] Changsheng Cao,[a] Jian Zhang[a] and Lei Zhang *[a]

Received 8th December 2021
Accepted 1st February 2022

DOI: 10.1039/d1sc06847d

rsc.li/chemical-science

Herein, we report the stepwise assembly and reversible transformation of atomically precise ligated titanium coated bismuth-oxide core nanostructures. The soluble and stable $Bi_{38}O_{45}$@Ti_6-oxo clusters with weakly coordinated surface salicylate ligands were first prepared as precursors. Owing to the high surface reactivity of the $Bi_{38}O_{45}$ inner core, its shell composition and morphology could be systemically modified by assembly with various Ti ions and auxiliary ligands (L), especially those with different flexibility, bridging ability and steric hindrance. As a result, a series of new core–shell $Bi_{38}O_{44/45}$@Ti_xL-oxo (x = 14, 16, 18 or 20) clusters containing gradually increasing shell Ti atoms were successfully synthesized. Among them, the $Bi_{38}Ti_{20}$-oxo cluster is the largest one in the family of heterometallic Bi/Ti-oxo clusters to date. In addition, the sensitized titanium outer shell can effectively improve the photocurrent response under visible light irradiation. More remarkably, the obtained core–shell $Bi_{38}O_{44/45}$@Ti_xL-oxo clusters can serve as stable and efficient catalysts for CO_2 cycloaddition with epoxides under ambient conditions, whose activity was significantly influenced by the outer ligated titanium shell structure. This work provides a new insight into the construction of atomically precise heterometallic core–shell nanostructures and also an interesting shell engineering strategy for tuning their physicochemical properties.

Introduction

Core–shell nanostructures have attracted a lot of research interest in chemical and materials science due to their improved physicochemical performances in comparison with individual components.[1,2] In particular, the active interfaces between the inner core and outer shell layers can facilitate outstanding synergistic functions to provide a variety of novel applications in catalysis, batteries, supercapacitors and photonics.[3–6] In the past few decades, there have been numerous core–shell structured materials reported, including metal nanoparticles as typical cores and metal oxides or porous carbon as major shells.[7,8] However, the majority of known core–shell structures belong to atomically heterogenous nanosized materials. It is rather difficult to determine and control their precise structures and compositions at the atomic level, which are crucial to the understanding of the structure–activity relationship.[9] Therefore, the construction of atomically precise core–shell nanostructures is quite appealing to better achieve the future rational design and performance optimization.[10–16]

As the molecular models of functional metal oxides, atomically precise metal-oxo clusters recently became a prominent research topic.[17,18] A growing number of interesting oxo clusters have been prepared, including representative complexes of Mo,[19] W,[20,21] V,[22] Nb,[23] Ti,[24–26] Sn,[27] Pd[28,29] and so on. The construction of metal-oxo clusters not only provides opportunities for mechanism research, but also sometimes brings unprecedented functionalities.[30,31] Moreover, the precise structural information of metal-oxo clusters also makes it possible to utilize them to construct atomically accurate core–shell structures. Indeed, we have just successfully used hollow titanium-oxo clusters to encapsulate and stabilize silver nanoclusters, resulting in several core–shell Ag_n@Ti_m-oxo structures.[32,33] Therefore, by changing the core/shell compositions, there will be a very broad space to build metal-oxo cluster-based core–shell nanostructures.

On the other hand, it has been well confirmed that the construction of metal oxide heterojunctions, *e.g.* Bi_2O_3–TiO_2,

[a]*State Key Laboratory of Structural Chemistry, Fujian Institute of Research on the Structure of Matter, Chinese Academy of Sciences, Fuzhou, Fujian 350002, P. R. China. E-mail: Lzhang@fjirsm.ac.cn*

[b]*University of Chinese Academy of Sciences, Chinese Academy of Sciences, Beijing 100049, P. R. China*

† Electronic supplementary information (ESI) available. CCDC 2104507, 2104508, and 2104511–2104515. For ESI and crystallographic data in CIF or other electronic formats see DOI: 10.1039/d1sc06847d

can dramatically improve their catalytic activities.[34] Accordingly, no matter from the perspective of new structures or new functions, molecular Bi_nO_x@Ti_mO_y core–shell nanostructures would be of great research value. Unfortunately, although both Bi- and Ti-oxo clusters are widely reported and bismuth was ever applied to stabilize Ti-oxo sulfate clusters by Nyman and co-workers,[17,24,35–38] the core–shell assembly between them is still quite challenging.

Recently, we have found that the $Ti(SAC)_3$ (H_2SAC = salicylic acid) moieties can act as versatile metalloligands to stabilize Ag clusters.[39] Similarly, these $Ti(SAC)_3$ species might also be applied to coat multinuclear Bi-oxo cores to form the desired core–shell nanostructures. Following this consideration, herein we successfully prepared the first core–shell Bi–Ti oxo cluster, $[Ti_6Bi_{38}O_{45}(SAC)_{18}(HSAC)_{12}]\cdot 2(H_2O)\cdot 4(NBA)\cdot 11(DMF)$ (NBA = 1-butanol) (**PTC-281**). Single crystal X-ray diffraction analysis indicates that **PTC-281** contains a $Bi_{38}O_{45}$ core which is surrounded by 12 weakly coordinated HSAC ligands and six $Ti(SAC)_3$ moieties. More interestingly, the shell of **PTC-281** has high surface reactivity, making it an ideal candidate for the stepwise assembly of core–shell $Bi_{38}O_{45}$@Ti_xL-oxo structures with different numbers of shell titanium atoms (Scheme 1). Thereupon, another six $Bi_{38}O_{44/45}$@Ti_xL-oxo clusters with 14, 16, 18 and 20 titanium atoms and various auxiliary ligands (L) surrounding the Bi_{38}-oxo core were successfully synthesized (Table 1). In addition, interesting reversible structural transformation has been discovered between some $Bi_{38}O_{44}$@Ti_xL-oxo clusters, further confirming the shell modifiability of these core–shell structures. Finally, the sensitized Ti shells result in different visible-light driven photocurrent responses and distinct catalytic activities towards the coupling reaction of epoxides with CO_2.

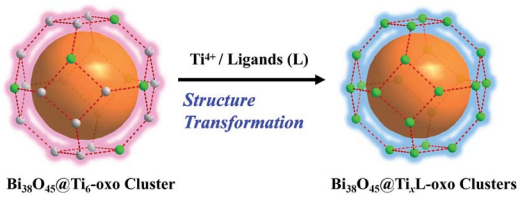

Scheme 1 Stepwise assembly of core–shell $Bi_{38}O_{44/45}$@Ti_xL-oxo cluster structures.

Results and discussion

Yellow crystals of **PTC-281** were synthesized by the reaction of bismuth subsalicylate, salicylic acid and $Ti(O^iPr)_4$ in a mixed DMF and NBA solution at 80 °C for three days. Single-crystal X-ray diffraction (SXRD) analysis revealed that **PTC-281** crystallized in a triclinic $P\bar{1}$ space group. The core structure of **PTC-281** is similar to the previously reported bismuth-oxo clusters, $[Bi_{38}O_{45}(hfac)_{24}]$ (Hhfac = hexafluoroacetylacetone)[40] and $[Bi_{38}O_{44}(HSAC)_{26}(Me_2CO)_{16}(H_2O)_2]\cdot(Me_2CO)_4$.[41] As shown in Fig. 1, the 38 bismuth atoms from the $Bi_{38}O_{45}$ inner core of **PTC-281** form a triple nested structure, Bi_6@Bi_8@Bi_{24}. Thus, the outermost Bi_{24} is a twisted truncated octahedron consisting of eight hexagonal {Bi_6} planes and six quadrilateral {Bi_4} planes. Among them, six hexagonal {Bi_6} planes are each coordinated by a $Ti(SAC)_3$ metalloligand with calixarene-like arrangement filled by coordination-active oxygen sites (Fig. S2†), and the remaining two {Bi_6} planes are each coordinated by three HSAC ligands. Meanwhile, all six {Bi_4} planes are each capped by one HSAC ligand. In order to clarify the position relationship between the outer shell Ti atoms and $Bi_{38}O_{45}$ inner core, an unfolded diagram of the Bi_{24} truncated octahedron is also given in Fig. 1. Clearly, six Ti atoms are each distributed on the hexagonal planes of the expanded truncated octahedron. The Ti and Bi components were further confirmed by inductively coupled plasma (ICP) analysis (Table S5†).

The crystals of **PTC-281** exhibit good solubility in DMF solvent with a saturated solubility of 12.5 g L^{-1} at 80 °C. Interestingly, a yellow rod-like crystal could be obtained in one day, named **PTC-281R** (Fig. S4†), after cooling to room temperature. X-ray diffraction analysis indicated that **PTC-281R** presented the same $Bi_{38}O_{45}$@Ti_6 structure as **PTC-281**, confirming the high solution stability of the clusters in **PTC-281**. In addition, scale up synthesis of **PTC-281** was realized by increasing the amounts of reactants (>25 g, Fig. S5†), which could provide sufficient samples for the subsequent stepwise assembly studies.

Based on the excellent solubility and stability of the $Bi_{38}O_{45}$@Ti_6 clusters in organic solvents, their stepwise assembly with additional titanium ions and different auxiliary ligands was then investigated. At the beginning, salicylic acid, piperazine and $Ti(O^iPr)_4$ were added to the DMF/EAC solution of **PTC-281**, which was then heated at 80 °C for one night,

Table 1 Summary of the formulae and core–shell compositions of PTC-281 to PTC-286[a]

			Shell	
Complex	Formula	Core	$Ti(SAC)_3$	Others components
PTC-281	$[Ti_6Bi_{38}O_{45}(SAC)_{18}(HSAC)_{12}]\cdot 2(H_2O)\cdot 4(NBA)\cdot 11(DMF)$	$Bi_{38}O_{45}$	6	12× HSAC
PTC-282	$H_2[Ti_{14}Bi_{38}O_{50}(SAC)_{30}(EtO)_{12}]\cdot 12(DMF)$	$Bi_{38}O_{44}$	2	6× $[Ti_2O(SAC)_4(EtO)_2]$
PTC-283	$[Ti_{16}Bi_{38}O_{51}(SAC)_{28}(HSAC)_2(DEA)_4(PhO)_{10}]\cdot 2(CH_3CN)$	$Bi_{38}O_{45}$	2	2× $[Ti_3O(SAC)_5(DEA)(PhO)_2]$; 2× $[Ti_4O(SAC)_6(DEA)(PhO)_3]$
PTC-284	$[Ti_{16}Bi_{38}O_{44}(SAC)_{34}(DPC)_6(PhO)_8]\cdot 4(CH_3CN)$	$Bi_{38}O_{44}$	2	2× $[Ti_3(SAC)_6(DPC)_2(PhO)]$; 2× $[Ti_4(SAC)_8(DPC)(PhO)_3]$
PTC-285	$[Ti_{18}Bi_{38}O_{50}(SAC)_{24}(DTPP)_6(DMT)_6][O^iPr]_2\cdot 12(DMF)$	$Bi_{38}O_{44}$	6	6× $[Ti_2O(SAC)(DTPP)(DMT)]$
PTC-286	$H_2[Ti_{20}Bi_{38}O_{50}(SAC)_{30}(DTPP)_6(CH_3O)_{12}]\cdot 4(DMF)$	$Bi_{38}O_{44}$	8	6× $[Ti_2O(SAC)(DTPP)(CH_3O)_2]$

[a] Abbreviations: HNBA = 1-butanol; PhOH = phenol; DMF = dimethylformamide; H_2DEA = diethanolamine; H_2DPC = *cis*-4-cyclohexene-1,2-dicarboxylic acid; H_4DTPP = di(trimethylolpropane); H_2DMT = 2,2′-biphenol.

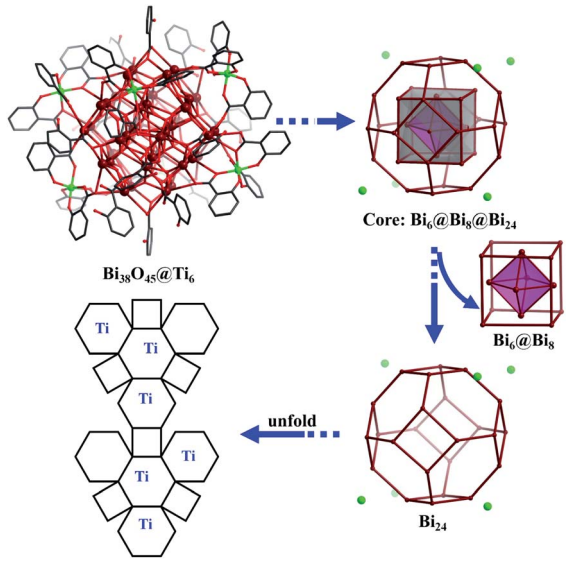

Fig. 1 Molecular structure and structural evolution with unfolded diagrams of PTC-281. Color codes: dark red Bi; green Ti; black C; red O. H atoms are omitted for clarity.

forming yellow block crystals of **PTC-282** (Fig. 2). Structural analysis revealed that **PTC-282** also contains a similar $Bi_{38}O_{44}$ cluster inner core, but 8 more Ti atoms are present in the outer shell. Different from **PTC-281**, in the structure of **PTC-282**, 24 SAC ligands are completely deprotonated to coordinate to form 12 $Ti(SAC)_2$ moieties, and then further connected together by a μ_3-O atom and one μ_2-EtO molecule to form a binuclear $[Ti_2O(SAC)_4(EtO)_2]$ unit (Fig. S6a†). As shown in Fig. 3, six such $[Ti_2O(SAC)_4(EtO)_2]$ units decorate six $\{Bi_6\}$ hexagons, and the remaining two $\{Bi_6\}$ planes are occupied by two $Ti(SAC)_3$ metalloligands, giving rise to the total $6 \times 2 + 2 = 14$ Ti atoms.

To capture more Ti atoms in the outer shell, the steric hindrance and bridging ability of the surface ligands should be considered. Therefore, more $Bi_{38}O_{45}$@Ti_xL-oxo assembly procedures were studied by selecting small flexible ligands with

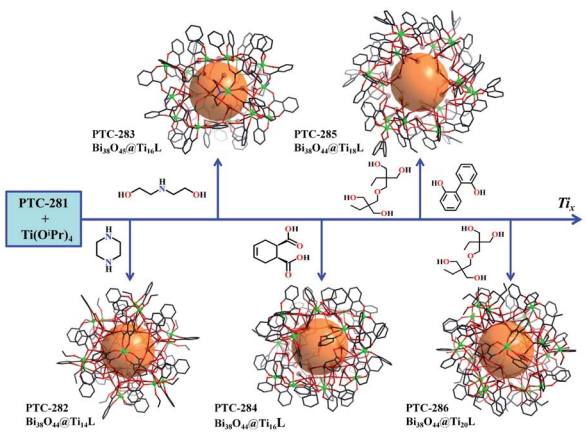

Fig. 2 Reaction scheme of the stepwise assembly from PTC-281 to the $Bi_{38}O_{44/45}$@Ti_xL-oxo cluster family, highlighting the outer shell molecular compositions of PTC-282 to PTC-286.

polyhydroxy groups. Following this idea, the diethanolamine (DEA) ligand was introduced into the reaction of salicylic acid and $Ti(O^iPr)_4$ in a CH_3CN/phenol solution of **PTC-281**, giving rise to **PTC-283** (Fig. 2). Compared with **PTC-282**, two more Ti atoms were incorporated, increasing the shell composition of **PTC-283** to 16 titanium atoms. The shell structure of **PTC-283** is composed of three kinds of subunits: two $Ti(SAC)_3$ metalloligands, two trinuclear $[Ti_3O(SAC)_5(DEA)(PhO)_2]$ moieties and two tetranuclear $[Ti_4O(SAC)_6(DEA)(PhO)_3]$ moieties, all of which are symmetrically distributed (Table 1 and Fig. S7†). It's worth noting that the $\{Ti_3\}$ subunit appears in a triangular arrangement across three adjacent planes (two $\{Bi_6\}$ and one $\{Bi_4\}$), while the $\{Ti_4\}$ subunit is arranged in a Z shape across four adjacent planes (three $\{Bi_6\}$ and one $\{Bi_4\}$) (Fig. 3).

In addition, when *cis*-4-cyclohexene-1,2-dicarboxylic acid (H_2DPC) was applied instead of DEA, red crystals of **PTC-284** were synthesized, whose shell also contains 16 Ti atoms (Table 1 and Fig. S9†). Interestingly, a Ti^{3+} ion was found in the structure of **PTC-284**, as confirmed by bond valence sum calculation studies and a strong signal at $g = 1.98$ in the ESR spectrum (Table S4 and Fig. S10†).[42] There are 48 surface ligands in the shell of **PTC-284**, which are more than the 30 surface ligands for **PTC-280**, 32 surface ligands for **PTC-281**, 42 surface ligands for **PTC-282** and 44 surface ligands for **PTC-283** (Table 1). Therefore, in order to accommodate these ligands, as shown in Fig. 3, all the titanium atoms in **PTC-284** were shifted to the edges of the hexagonal $\{Bi_6\}$ planes and quadrilateral $\{Bi_4\}$ planes.

It is interesting that when larger DTPP and DMT ligands were simultaneously used, **PTC-285** was obtained whose outer shell holds 18 Ti atoms and 42 surface ligands (Fig. 2 and Table 1). Due to the steric hindrance of the larger DTPP and DMT ligands, the arrangement of Ti atoms in **PTC-285** is quite unique, with six binuclear $[Ti_2O(SAC)(DTPP)(DMT)]$ units anchored to the six quadrilateral $\{Bi_4\}$ planes of the $Bi_{38}O_{44}$ core in a head-to-head fashion (Fig. S12a†), while, the Ti atoms in **PTC-280** to **PTC-284** all adopt a side-by-side fashion. Herein, the head-to-head anchored fashion in **PTC-285** makes one Ti atom from the binuclear unit protrude out of the $\{Bi_4\}$ plane to overcome the steric hindrance effect (Fig. 3). In addition, there are six more $Ti(SAC)_3$ metalloligands to coordinate six hexagonal $\{Bi_6\}$ planes, forming the total $6 \times 2 + 6 = 18$ Ti atoms in the outer shell of **PTC-285**. It is worth noting that there are still two $\{Bi_6\}$ planes unoccupied by any ligands, showing the potential to accommodate more Ti atoms.

Fortunately, yellow block crystals of **PTC-286** with two more shell Ti atoms were obtained by using less methanol instead of DMT (Fig. 2). As expected, the shell of **PTC-286** is similar to that of **PTC-285**, with six quadrilateral $\{Bi_4\}$ planes also anchored by six binuclear $[Ti_2O(SAC)(DTPP)(CH_3O)_2]$ units in a head-to-head fashion (Fig. S13†). Attributed to the weakening of the steric hindrance effect in the outer shell, all eight hexagonal $\{Bi_6\}$ planes of **PTC-286** are coordinated by $Ti(SAC)_3$ metalloligands, giving rise to the total $6 \times 2 + 8 = 20$ Ti atoms in the shell.

From the above results, the robustness of the Bi_{38}-oxo inner core and the variability of its outer shell composition have been clearly confirmed. Such unique characteristics might also

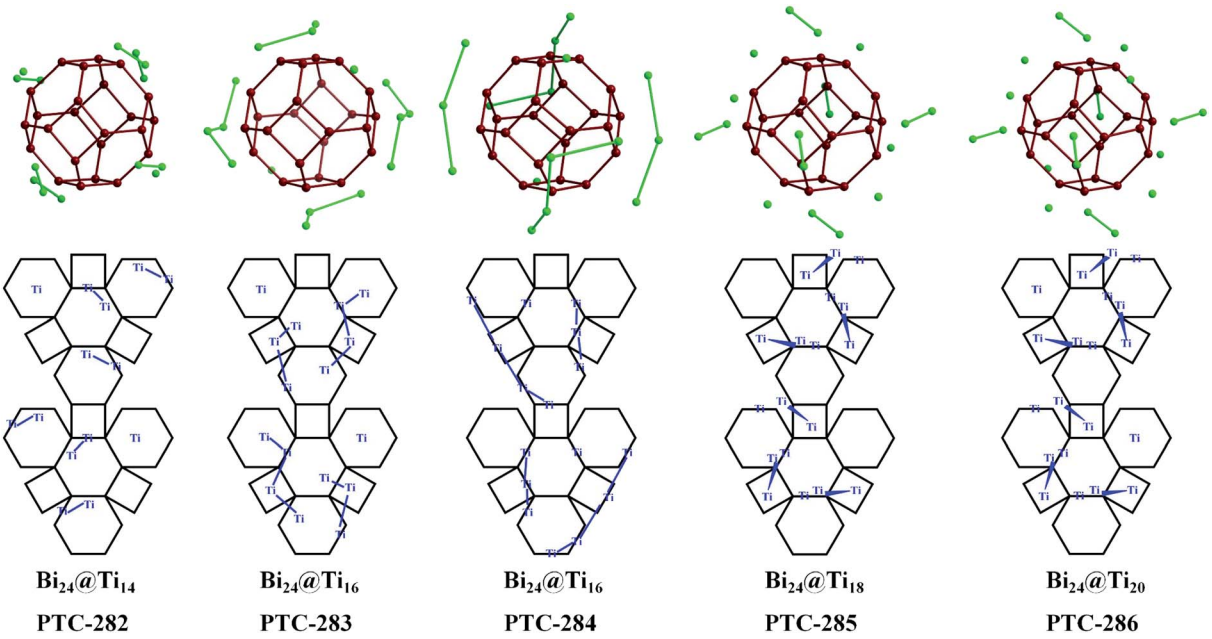

Fig. 3 Structural distribution of Ti atoms on the surface of the Bi_{38}-oxo inner core in **PTC-282** to **PTC-286**. Unfolded diagrams are also provided to better illustrate their relative position. The green line shows Ti atoms that are bridged together by μ_2-O atoms or ligands.

produce post-synthetic structural transformation between the obtained $Bi_{38}O_{44}$@Ti_xL-oxo core–shell clusters. To further verify this point, the assembly behavior of **PTC-284** was studied (Fig. 4). A series of stepwise assembly reactions of **PTC-284** were carried out, giving rise to crystals with structures of **PTC-282**, **PTC-285** and **PTC-286** (Fig. S15c, S16b and c†). More interestingly, some of these structural transformations are reversible, like those between **PTC-284** and **PTC-282** (Fig. S16a†), while, the transformations from **PTC-284** to **PTC-285** and **PTC-286** only happen in one direction. Such differences might be attributed to the different coordination abilities of the corresponding auxiliary ligands. These results fully confirm that the obtained $Bi_{38}O_{44}$@Ti_xL-oxo core–shell clusters have very rich assembly chemistry, which could be used as versatile platforms for new structures and functionalities.

The solid-state UV-vis absorption spectra of these complexes display intense absorption in the visible region, and the calculated optical bandgaps are in the range from 2.00 eV to 2.34 eV (Fig. S20 to S22†). Based on these results, the visible-light driven photocurrent responses of the $Bi_{38}O_{44/45}$@Ti_xL-oxo core–shell clusters were measured, and the measurements were carried out in a 0.20 mol L^{-1} Na_2SO_4 electrolyte solution under on-off cycling irradiation by UV-vis light with a 420 nm cutoff filter

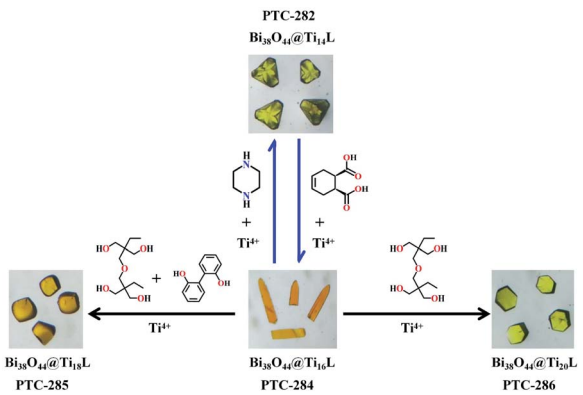

Fig. 4 Reversible or one-way transformation scheme between **PTC-284** and **PTC-282**, **PTC-285**, **PTC-286**.

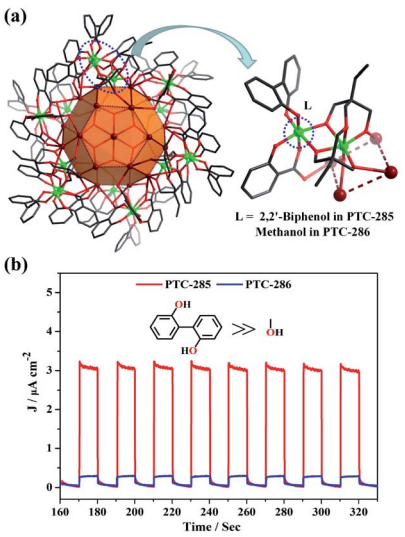

Fig. 5 (a) Structural illustration of **PTC-286**, highlighting the shell $[Ti_2(\mu_3\text{-O})(SAC)(DTPP)(CH_3O)_2]$ unit with two methanol molecules that can be replaced by one DMT ligand in **PTC-285**; (b) transient photocurrent responses of **PTC-285** and **PTC-286** under visible light irradiation in 0.2 M Na_2SO_4 electrolyte solution.

(intervals of 10 s). As shown in Fig. 5b and S23,† upon repetitive irradiation, steady photocurrent responses were observed for all the complexes used. Notably, for **PTC-285** and **PTC-286** with the same DTPP ligand, when the surface methanol molecules were replaced by the DMT ligand (Fig. 5a), the photocurrent density greatly increased (Fig. 5b). Thus, **PTC-285** (DMT) exhibited the optimal photocurrent response among all the $Bi_{38}O_{44/45}$@Ti_xL-oxo clusters, and its current density value reached 3.23 μA cm^{-2} which was about 11.54 times that of **PTC-286** (methanol, 0.28 μA cm^{-2}). Therefore, the DMT ligand can be considered as more photosensitive to better harvest visible light.[24]

It is worth mentioning that some Bi atoms in the above $Bi_{38}O_{44/45}$@Ti_xL core–shell clusters are exposed to the surface, *e.g.* the hexagonal {Bi_6} planes in **PTC-285**, making them possible Lewis acid sites for catalytic reactions (Fig. 6a).[43] To explore this hypothesis, the transformation of CO_2 with epoxides was chosen as a model reaction. The experiments were carried out at room temperature and 1 atm pressure in the presence of a 0.5 mol‰ catalyst combined with tetrabutylammonium bromide, and the yields of these compounds range from 63% to 86%, indicating that they exhibit different catalytic activities. Among them, **PTC-285** with exposed {Bi_6} sites indeed showed the best yield of 86% (Table 2, entry 1). As for **PTC-286** with a deeply embedded $Bi_{38}O_{44}$ inner core and all occupied {Bi_6} planes (Fig. 6b), it should be more difficult to expose surface Bi sites, producing a much lower yield than **PTC-285** (Table 2, entry 6). Therefore, the outer shell structures of the $Bi_{38}O_{44/45}$@Ti_xL clusters have significant influence on their catalytic activities towards chemical CO_2 fixation.

To further explore optimal catalytic performance and acquire some mechanistic information, **PTC-285** and **PTC-286** were selected as representatives for detailed studies. It was reported that the conversion of epoxides into cyclic carbonates could be effectively improved by increasing the reaction temperature and pressure or prolonging the reaction time.[44–47] Indeed, although carried out under room temperature and 1 atm pressure, the yields of propylene carbonate and 1,2-butylene carbonate by **PTC-285** could still be increased to 99% and 95% by prolonging the reaction time to 48 hours (Table 3, entry 1, 3). In addition, the size effect of the substrate was investigated. When the larger styrene oxide was applied, **PTC-285** showed lower catalytic activity to give only 60% yield of phenylethylene carbonate (Table 3, entry 5); while with the largest substrate of cyclohexene oxide, the lowest product yield of 30% was obtained (Table 3, entry 7). Such an obvious steric effect further indicates that the epoxide substrates used need to go through the Ti_xL outer shell to approach the Bi active sites on the inner Bi_{38}-oxo core. Correspondingly, lower yields were observed for larger substrates due to steric hindrance.

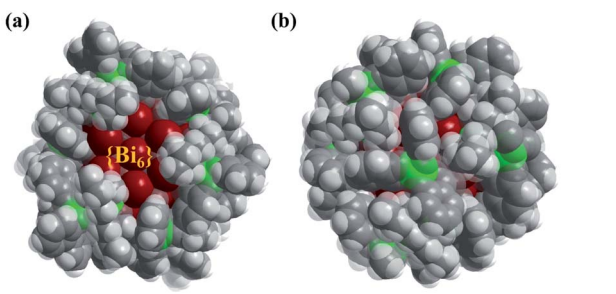

Fig. 6 (a) Space-filling model of the structure of **PTC-285**, highlighting the exposed {Bi_6} active sites; (b) space-filling model of the structure of **PTC-286**. Color codes: green Ti; dark red Bi; gray C and O; white H.

Table 2 Screening of the synthesis of cyclic carbonate from CO_2 and epichlorohydrin using $Bi_{38}O_{44/45}$@Ti_xL-oxo core–shell clusters as catalysts[a]

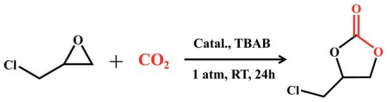

Entry	Catalyst	Yield[b] (%)
1	**PTC-285**	86
2	**PTC-282**	84
3	**PTC-281**	76
4	**PTC-284**	75
5	**PTC-283**	70
6	**PTC-286**	63
7	**Blank**	44

[a] Reaction conditions: epichlorohydrin (10 mmol), catalysts (0.005 mmol), nBu_4NBr (1 mmol), room temperature, 24 h, CO_2 (1 atm gauge pressure). [b] Total yield was determined by ^1H NMR spectroscopy using dibromomethane as an internal standard (Fig. S31 to S36).

Table 3 The catalytic coupling of different epoxides with CO_2 using **PTC-285** and **PTC-286** as catalysts[a]

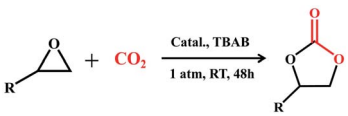

Entry	Catalyst	Epoxides	Products	Yield[b] (%)
1	**PTC-285**			99
2	**PTC-286**			62
3	**PTC-285**	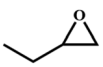	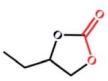	95
4	**PTC-286**			60
5	**PTC-285**	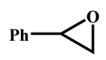	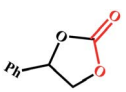	60
6	**PTC-286**			32
7	**PTC-285**		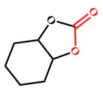	30
8	**PTC-286**			10

[a] Reaction conditions: epoxides (10 mmol), catalysts (0.005 mmol), nBu_4NBr (1 mmol), room temperature, 48 h, CO_2 (1 atm gauge pressure). [b] Total yield was determined by ^1H NMR spectroscopy using dibromomethane as an internal standard (Fig. S37 to S44).

Moreover, as shown in Table 3, when **PTC-285** was replaced by **PTC-286**, the yields of all four carbonates were greatly reduced, further indicating that the catalytic activity of **PTC-285** is much better than that of **PTC-286**. From the above structural analysis, the most significant difference between **PTC-285** and **PTC-286** is that **PTC-285** holds surface exposed $\{Bi_6\}$ sites. Therefore, these results further confirm the effect of shell morphology on the catalytic activities.

The catalytic stability of the $Bi_{38}O_{44/45}$@Ti_xL-oxo core–shell clusters used was also studied. The solution-state UV-vis spectra and solid-state IR spectra of these catalysts before and after catalytic studies were basically unchanged (Fig. S25 to S29†). Furthermore, the sample of **PTC-285** could be reused three successive times which maintained its catalytic performance to a large extent (Fig. S30†). These results demonstrated the high stability of the applied $Bi_{38}O_{44/45}$@Ti_xL-oxo cluster catalysts.

According to the reported mechanism of the cycloaddition of epoxides with CO_2,[43,48] we also proposed a tentative reaction mechanism for our studies (Fig. S30†). First, epoxides are activated by the exposed Lewis acidic Bi sites in the Bi_{38}-oxo inner core. Subsequently, Br^- from TBAB attacks the coordinated epoxide to promote its ring opening effectively. Finally, CO_2 around the active sites attacks the activated C atom and Br^- is removed to complete the catalytic reaction.

Conclusions

In summary, a core–shell $Bi_{38}O_{45}$@Ti_6-oxo cluster with high solubility and solution stability in organic solvents was prepared and applied as a versatile precursor for the stepwise assembly of a series of $Bi_{38}O_{44/45}$@Ti_xL-oxo core–shell nanostructures. Attributed to its high surface reactivity, the outer ligated titanium shell composition has been successfully increased to 14, 16, 18 and 20 Ti atoms with the assistance of auxiliary ligands with different flexibility, coordination behavior and geometric effects. Furthermore, interesting reversible structural transformation has been realized between some $Bi_{38}O_{44}$@Ti_xL-oxo clusters, further confirming the shell modifiability of these core–shell structures. In addition, the sensitized Ti outer shell showed a great effect on their physicochemical properties, including excellent visible-light driven photocurrent responses and enhanced catalytic activities for the coupling reaction between epoxides and CO_2 under normal temperature and pressure. Especially, the outer ligated titanium shell structures determined the exposure degree of Bi active sites and shuttle behavior of epoxide substrates, resulting in steric hindrance dependent product yields. Therefore, an effective stepwise strategy has been successfully established for the assembly of atomically precise Bi_nO_x@Ti_mO_y core–shell nanostructures, which could be extended to the construction of more core–shell materials with tunable composition and optimizable applications.

Data availability

All experimental supporting data and procedures are available in the ESI.†

Author contributions

L. Z. designed the study and supervised the project. Q. D., Y. Y., and C. C. performed the experiments. All the authors discussed the results and co-wrote the manuscript.

Conflicts of interest

There are no conflicts to declare.

Acknowledgements

This work was supported by the National Natural Science Foundation of China (21922111 and 91961108).

Notes and references

1 R. G. Chaudhuri and S. Paria, *Chem. Rev.*, 2012, **112**, 2373–2433.
2 S. Das, J. Pérez-Ramírez, J. Gong, N. Dewangan, K. Hidajat, B. C. Gates and S. Kawi, *Chem. Soc. Rev.*, 2020, **49**, 2937–3004.
3 C. Xie, Z. Niu, D. Kim, M. Li and P. Yang, *Chem. Rev.*, 2020, **120**, 1184–1249.
4 Z. Yi, Q. Han, P. Zan, Y. Cheng, Y. Wu and L. Wang, *J. Mater. Chem. A*, 2016, **4**, 12850–12857.
5 M. Wang, Z. Li, C. Wang, R. Zhao, C. Li, D. Guo, L. Zhang and L. Yin, *Adv. Funct. Mater.*, 2017, **27**, 1701014–1701023.
6 D. Huo, M. J. Kim, Z. Lyu, Y. Shi, B. J. Wiley and Y. Xia, *Chem. Rev.*, 2019, **119**, 8972–9073.
7 X. Liu, J. Iocozzia, Y. Wang, X. Cui, Y. Chen, S. Zhao, Z. Li and Z. Lin, *Energy Environ. Sci.*, 2017, **10**, 402–434.
8 X. Xia, Y. Zhang, Z. Fan, D. Chao, Q. Xiong, J. Tu, H. Zhang and H. J. Fan, *Adv. Energy Mater.*, 2014, 1401709–1401717.
9 C. Hu, R. Chen and N. Zheng, *Adv. Mater.*, 2021, 2006159–2006168.
10 X.-K. Wan, X.-L. Cheng, Q. Tang, Y.-Z. Han, G. Hu, D. Jiang and Q.-M. Wang, *J. Am. Chem. Soc.*, 2017, **139**, 9451–9454.
11 Z. Wang, H.-F. Su, C.-H. Tung, D. Sun and L.-S. Zheng, *Nat. Commun.*, 2018, **9**, 4407–4417.
12 H. Yang, J. Zhang, M. Luo, W. Wang, H. Lin, Y. Li, D. Li, P. Feng and T. Wu, *J. Am. Chem. Soc.*, 2018, **140**, 11189–11192.
13 K. Yonesato, H. Ito, H. Itakura, D. Yokogawa, T. Kikuchi, N. Mizuno, K. Yamaguchi and K. Suzuki, *J. Am. Chem. Soc.*, 2019, **141**, 19550–19554.
14 X. Kang, Y. Li, M. Zhu and R. Jin, *Chem. Soc. Rev.*, 2020, **49**, 6443–6514.
15 S.-Z. Zhan, G.-H. Zhang, J.-H. Li, J.-L. Liu, S.-H. Zhu, W. Lu, J. Zheng, S. W. Ng and D. Li, *J. Am. Chem. Soc.*, 2020, **142**, 5943–5947.
16 Y. Jin, C. Zhang, X.-Y. Dong, S.-Q. Zang and T. C. W. Mak, *Chem. Soc. Rev.*, 2021, **50**, 2297–2319.
17 W.-H. Fang, L. Zhang and J. Zhang, *Chem. Soc. Rev.*, 2018, **47**, 404–421.
18 N. I. Gumerova and A. Rompel, *Chem. Soc. Rev.*, 2020, **49**, 7568–7601.

19 H. N. Miras, G. J. T. Cooper, D.-L. Long, H. Bogge, A. Muller, C. Streb and L. Cronin, *Science*, 2010, **327**, 72–74.
20 C.-H. Zhan, R. S. Winter, Q. Zheng, J. Yan, J. M. Cameron, D.-L. Long and L. Cronin, *Angew. Chem., Int. Ed.*, 2015, **127**, 14516–14520.
21 S. An, J. C. Liu, H. Zhang, L. Wu and Y. F. Song, *Sci. China: Chem.*, 2019, **62**, 159–161.
22 L. K. Mahnke, A. Kondinski, U. Warzok, C. Näther, J. Leusen, C. A. Schalley, K. Yu. Monakhov, P. Kçgerler and W. Bensch, *Angew. Chem., Int. Ed.*, 2018, **57**, 2972–2975.
23 Y.-L. Wu, X.-X. Li, Y.-J. Qi, H. Yu, L. Jin and S.-T. Zheng, *Angew. Chem., Int. Ed.*, 2018, **57**, 8572–8576.
24 Q.-Y. Zhu and J. Dai, *Coord. Chem. Rev.*, 2021, **430**, 213664–213676.
25 N. Li, J. Liu, J.-J. Liu, L.-Z. Dong, S.-L. Li, B.-X. Dong, Y.-H. Kan and Y.-Q. Lan, *Angew. Chem., Int. Ed.*, 2019, **58**, 17260–17264.
26 C. Zhao, Y.-Z. Han, S. Dai, X. Chen, J. Yan, W. Zhang, H. Su, S. Lin, Z. Tang, B. K. Teo and N. Zheng, *Angew. Chem., Int. Ed.*, 2017, **56**, 16252–16256.
27 S. Saha, D.-H. Park, D. C. Hutchison, M. R. Olsen, L. N. Zakharov, D. Marsh, S. Goberna-Ferrón, R. T. Frederick, J. T. Diulus, N. Kenane, G. S. Herman, D. W. Johnson, D. A. Keszler and M. Nyman, *Angew. Chem., Int. Ed.*, 2017, **56**, 10140–10144.
28 S. Bhattacharya, U. Basu, M. Haouas, P. Su, M. F. Espenship, F. Wang, A. Solé-Daura, D. H. Taffa, M. Wark, J. M. Poblet, J. Laskin, E. Cadot and U. Kortz, *Angew. Chem., Int. Ed.*, 2021, **60**, 3632–3639.
29 P. Yang and U. Kortz, *Acc. Chem. Res.*, 2018, **51**, 1599–1608.
30 X. Fan, J. Wang, K. Wu, L. Zhang and J. Zhang, *Angew. Chem., Int. Ed.*, 2019, **58**, 1320–1323.
31 G. Zhang, C. Liu, D.-L. Long, L. Cronin, C.-H. Tung, G. Zhang, W. Li, C. Liu, J. Jia, C.-H. Tung and Y. Wang, *J. Am. Chem. Soc.*, 2018, **140**, 66–69.
32 S. Chen, W.-H. Fang, L. Zhang and J. Zhang, *Angew. Chem., Int. Ed.*, 2018, **57**, 11252–11256.
33 X. Fan, F. Yuan, D. Li, S. Chen, Z. Cheng, Z. Zhang, S. Xiang, S.-Q. Zang, J. Zhang and L. Zhang, *Angew. Chem., Int. Ed.*, 2021, **60**, 12949–12954.
34 M. Ge, C. Cao, S. Li, S. Zhang, S. Deng, J. Huang, Q. Li, K. Zhang, S. S. Al-Deyab and Y. Lai, *Nanoscale*, 2015, **7**, 11552–11560.
35 M. Mehring, *Coord. Chem. Rev.*, 2007, **251**, 974–1006.
36 K. Chintakrinda, N. Narayanam, Y.-Z. Li, F. Wang, C. Kashi, Q.-H. Li, G. Xu, L. Zhang and J. Zhang, *CCS Chem.*, 2020, **2**, 209–215.
37 J. C. Liu, Q. Han, L. J. Chen, J. W. Zhao, C. Streb and Y. F. Song, *Angew. Chem., Int. Ed.*, 2018, **57**, 8416–8420.
38 P. I. Molina, K. Kozma, M. Santala, C. Falaise and M. Nyman, *Angew. Chem., Int. Ed.*, 2017, **56**, 16277–16281.
39 M.-Y. Gao, K. Wang, Y. Sun, D. Li, B.-Q. Song, Y. H. Andaloussi, M. J. Zaworotko, J. Zhang and L. Zhang, *J. Am. Chem. Soc.*, 2020, **142**, 12784–12790.
40 E. V. Dikarev, H. Zhang and B. Li, *Angew. Chem., Int. Ed.*, 2006, **45**, 5448–5451.
41 P. C. Andrews, G. B. Deacon, C. M. Forsyth, P. C. Junk, I. Kumar and M. Maguire, *Angew. Chem., Int. Ed.*, 2006, **45**, 5638–5642.
42 J. Wang, Y. Wang, W. Wang, T. Peng, J. Liang, P. Li, D. Pan, Q. Fan and W. Wu, *Environ. Pollut.*, 2020, **262**, 114373–114383.
43 G. Zhai, Y. Liu, L. Lei, J. Wang, Z. Wang, Z. Zheng, P. Wang, H. Cheng, Y. Dai and B. Huang, *ACS Catal.*, 2021, **11**, 1988–1994.
44 E. López-Maya, N. M. Padial, J. Castells-Gil, C. R. Ganivet, A. Rubio-Gaspar, F. G. Cirujano, N. Almora-Barrios, S. Tatay, S. Navalón and C. Martí-Gastaldo, *Angew. Chem., Int. Ed.*, 2021, **60**, 11868–11873.
45 H. Xu, C.-S. Cao, H.-S. Hu, S.-B. Wang, J.-C. Liu, P. Cheng, N. Kaltsoyannis, J. Li and B. Zhao, *Angew. Chem., Int. Ed.*, 2019, **58**, 6022–6027.
46 G. Li, X. Sui, X. Cai, W. Hu, X. Liu, M. Chen and Y. Zhu, *Angew. Chem., Int. Ed.*, 2021, **60**, 10573–10576.
47 X. M. Kang, Y. Shi, C. S. Cao and B. Zhao, *Sci. China: Chem.*, 2019, **62**, 622–628.
48 J. Dong, P. Cui, P.-F. Shi, P. Cheng and B. Zhao, *J. Am. Chem. Soc.*, 2015, **137**, 15988–15991.